Materials Science and Engineering C 78 (2017) 674–681

Contents lists available at ScienceDirect

Materials Science and Engineering C

journal homepage: www.elsevier.com/locate/msec

Drug release profiles of modified MCM-41 with superparamagnetic behavior correlated with the employed synthesis method

Natalia I. Cuello [a], Verónica R. Elías [a], Silvia N. Mendieta [a], Marcela Longhi [b], Mónica E. Crivello [a], Marcos I. Oliva [c], Griselda A. Eimer [a,*]

[a] Centro de Investigación y Tecnología Química (CITeQ) (UTN-CONICET), Facultad Regional Córdoba, Maestro López y Cruz Roja Argentina, Ciudad Universitaria, 5016 Córdoba, Argentina
[b] Unidad de Investigación y Desarrollo en Tecnología Farmacéutica, UNITEFA CONICET-UNC, Departamento de Farmacia, Facultad de Ciencias Químicas, Universidad Nacional de Córdoba, Ciudad Universitaria, 5000 Córdoba, Argentina
[c] Facultad de Matemática, Astronomía y Física, Universidad Nacional de Córdoba – IFEG, CONICET. Ciudad Universitaria, 5000 Córdoba, Argentina

ARTICLE INFO

Article history:
Received 14 June 2016
Received in revised form 13 October 2016
Accepted 6 February 2017
Available online 08 February 2017

Keywords:
Modified MCM-41
Superparamagnetism
Drug release
Indomethacin
Kinetic models

ABSTRACT

Mesoporous materials with superparamagnetic properties were successfully synthesized by two different methods: direct incorporation (DI) and wet impregnation (WI). The synthetized solids were evaluated as host of drugs for delivery systems and their physicochemical properties were characterized by XRD, ICP, N_2 adsorption-desorption, spectroscopies of UV–Vis DR, FT-IR and their magnetic properties were measured. Indomethacin (IND) was incorporated into the materials and the kinetic of the release profiles was studied by applying the Pepas and Sahlin model. In this sense, materials modified by DI, particularly that with hydrothermal treatment, showed the higher adsorption capacity and slower release rate. This behavior could be associated to the synthesis method used that allowed a high percentage of silanol groups available in the solids surface, which can interact with the IND molecule. This feature coupled with the superparamagnetic behavior; make these materials very interesting for drug delivery systems.

1. Introduction

In recent years, the field of nanotechnology has motivated researchers to develop nanostructured materials for human health care. In this sense, drug-delivery systems with magnetic properties are one of their most promising applications in the field of biomedical, materials science providing advantages over conventional drug therapies [1–4].

Mesoporous silica materials have been researched in order to develop very interesting drug-delivery systems. The literature shows many examples of drug molecules loaded onto mesoporous silica materials [5–7]. Particularly, MCM-41 is one of the most attractive porous materials because it possesses high specific surfaces (>900 m^2/g), tunable pore diameters (2–10 nm), high pore volumes and well organized porosity [8,9]. This huge surface available can lead to higher loading capacity of the drug, thus improving the dose of nanostructures needed as shuttle for the delivery. In addition, the thermal stability, and superior biocompatibility, has made these materials highly desirable in biomedical fields [10–14]. With respect to the biocompatibility, initial *in vitro* studies [15–17] demonstrated remarkable solubility of the mesoporous silica in simulated human plasma and other body fluids as those of the stomach, intestine, lung and/or urinary tract. This property is fundamental due to that the silica is not accumulated in the body; instead it is degraded and the products of its degradation are excreted through the kidneys [18]. In this context, it is pertinent to mention the synthesis of mesoporous composites having magnetic elements embedded in the nanochannels or in the porous framework as an alternative to the release of drugs. In this way, it is expected that, the drug loaded on carrier can be guided by an external magnetic field toward where it should be released, thus preventing its spread throughout the rest of the body.

Meanwhile, the size reduction of magnetic materials below a certain critical value, induces a magnetic transition where ferri-, ferromagnetic and antiferromagnetic nanoparticles become superparamagnetic. Thus, a reduction of the nanoparticles size is searched, due to that the magnetic parameters such as the coercivity can be finely tuned by decreasing the size of them. Moreover, these systems have high magnetic moments under the effect of a magnetic field, but they have not remanent magnetic moment when the external magnetic field is removed. This property is necessary especially *in vivo* experiments due to that the absence of net magnetic moment of the nanoparticles (zero coercivity) after concluding the diagnostic measurement or the therapy will prevent the potential aggregation of the particles that could easily cause the formation of embolisms in the blood vessels.

In this work, we have prepared drug-loaded samples using MCM-41 materials and drug release studies were carried out. Indomethacin

* Corresponding author.
E-mail addresses: geimer@frc.utn.edu.ar, griseeimer@yahoo.com.ar (G.A. Eimer).

http://dx.doi.org/10.1016/j.msec.2017.02.010
0928-4931/

(IND) is a nonsteroidal anti-inflammatory drug (NSAID) that reduces fever, pain and inflammation. This was chosen as the model drug for the release studies due to its hydrophobic character, similar to that of the substances used in chemotherapy. In fact, some studies have reported the chemo-preventive activity of non-steroidal anti-inflammatory drugs, including IND, against tumor cells [19–21]. Nonetheless, is a growing challenge for the pharmaceutical industry to find new routes to deliver this kind of drugs with hydrophobic character because they are poorly soluble in water and difficult to manage *via* the oral route. On the other hand, there are several mathematical models available in the literature to describe the drug release profile. The nature of the release profile largely depends on the textural properties of the host materials, such as pore diameters, pore volumes, particle morphology and surface modifications.

In this work a detailed study about the performance of superparamagnetic modified MCM-41 in IND-delivery systems has been made. In this way, the intrinsic relationship between their properties derived from synthesis methods and the release mechanism has been studied.

2. Experimental

2.1. Synthesis silica matrix

The MCM-41 type mesoporous molecular sieve was synthesized as previously reported [22].

2.2. Wet impregnation method (WI)

The MCM-41 host, previously calcined for 5 h in oven at 500 °C, was modified with Fe or Co using aqueous solution of several concentrations of the metal precursor. This synthesis method and the characterization of the obtained solids have been reported [23–24]. In this study, the sample corresponding to theoretical Fe loadings of 1 wt.% designated as Fe-WI(0.93) and the sample corresponding to theoretical Co loadings of 2.5 wt.% designated as Co-WI(2.20) have been tested like drug-delivery systems. The value in parentheses corresponds to experimental metal content in wt.%.

2.3. Direct incorporation method (DI)

The iron-containing MCM-41 type mesoporous materials were prepared by a direct hydrothermal method using cetyltrimethylammonium bromide (CTAB) as template, tetraethoxysilane (TEOS) as silicon source and ferric nitrate ($Fe(NO_3)_3 \cdot 9H_2O$) as metal precursor. The pH of the reaction mixture was adjusted to 12 by adding a 2 M sodium hydroxide (NaOH) aqueous solution. The catalysts were synthesized from a gel of molar composition: Si/Fe = 20; OH/Si = 0.5; CTAB/Si = 0.12; H_2O/Si = 132. In a typical synthesis, CTAB were dissolved in a NaOH solution in water under agitation at 40 °C. Then, TEOS and the metal source were added to this solution at 25 °C and the stirring was maintain for 4 h and then 3 h at 70 °C. Finally, this gel was filtered, washed with distilled water and dried at 60 °C overnight or treated hydrothermally under autogeneous pressure using a Teflon-lined stainless-steel autoclave, kept in an oven at 100 °C for 1 day. Again, the hydrothermally treated final solid were filtered, washed with distilled water until pH ~ 7 and dried at 60 °C overnight. The template was removed from the samples by heating (2 °C/min) under N_2 flow (45 mL/min) at 500 °C for 6 h and then calcinated at 500 °C for 6 h under dry air flow (45 mL/min). These samples were designated as Fe-DI(6.27) and Fe-DI(6.27)HT where the metal content in wt.% is indicated in brackets, "DI" indicates that the direct method was used and "HT" indicates that an hydrothermal treatment was applied.

2.4. Drug incorporation

Loading of Indomethacin within support was done by immersing the solid (0.150 g) into a highly concentrated ethanol solution of IND (0.450 g in 3 mL), which was mixed under stirring for 24 h in a thermostated bath at 68 °C. After the loading, the suspension was filtered and the resulting solid was dried in an oven at 36 °C. After incorporating IND in supports, samples were renamed as: Fe/WI(0.93)/IND, Co/WI(2.20)/IND, Fe-DI(6.27)/IND, Fe-DI(6.27)HT/IND and MCM-41/IND.

Finally, the loaded drug in the support was determined by extraction in ethanol of this, from a known amount of support-IND at 36 °C under stirring for 3 h. The extracted drug was measured by UV–Vis spectroscopy using the corresponding calibration curve obtained at $\lambda = 320$ nm (wavelength where IND has its maximum absorption). The amount of drug incorporated on the support is expressed in wt.% with respect to the loaded sample.

2.5. Drug release experiments

Drug release studies were performed in the dissolution apparatus Hanson Research SR6 serie II baskets type. The baskets rotation speed was 50 rpm and the vessels were kept in a thermostatically controlled circulation water bath at 37.0 ± 0.5 °C. The used dissolution media consisted of simulated body fluid [25] (SBF) at pH 7.4 ± 0.05, taking in mind a possible drug supply route *via* blood. A liter of this solution contained reagents added in amounts and order indicated as follow: 1) NaCl (8.036 g), 2) $NaHCO_3$ (0.325 g), 3) KCl (0.225 g), 4) K_2HPO_4 $3H_2O$ (0.230 g), 5) $MgCl_2$ $6H_2O$ (0,311 g), 6) 1 M HCl (40 mL), 7) $CaCl_2$ (0,293 g), 8) Na_2SO_4 (0,072 g), 9) 2-Amino-2-hydroxymethyl-1,3-propanediol (TRIS) (6063 g) and about 0,8 mL of HCl 1 M. The release studies were done by adding a known amount of IND in 750 mL of medium under sink conditions. Samples of 7 mL were withdrawn at predetermined intervals, followed by replenishment after each withdrawal with the same volume of fresh medium equilibrated at 37.0 ± 0.5 °C. Samples were appropriately filtered (filter type: 0.45 μm, Milipore 13 mm) and analyzed by UV absorption using a spectrophotometer Jasco 7800 at $\lambda = 320$ nm. The released drug amount at each time was expressed as a fraction of the total amount of IND. Drug release was monitored for 8 h; IND concentration was reported as an average of three determinations.

2.6. Characterization

X-ray diffraction patterns (XRD) were recorded in a Philips PW 3830 diffractometer with Cu Kα radiation ($\lambda = 1.5418$ Å) in the range of 2θ from 1.5° to 7° and from 20° to 80°. The specific surface, the pore size distribution, and the total pore volume were determined from N_2 adsorption-desorption isotherms obtained at −196 °C using a Micromeritics ASAP 2010. The surface was determined by the Brunauer-Emmet-Teller (BET) method in the pressure range of P/P_0: 0.01–0.21, while the pore sizes were determined by the NLDFT (Non-Local Density Functional) method [26]. The Fe content was measured by inductively coupled plasma optical emission spectroscopy (ICP) using a VISTA-MPX CCD Simultaneus ICP-OES-VARIAN. FT-IR spectral measurements were performed on a Jasco FT-IR 5300 spectrometer equipped with a DTGS detector. A self-supporting wafer for each sample (~20 mg and 13 mm of diameter) was prepared, placed in a thermostatized cell with CaF_2 windows connected to a vacuum line, and evacuated for 8 h at 400 °C in order to remove water adsorbed. The background spectrum was recorded first after cooling the sample to room temperature. UV–Vis diffuse reflectance (UV–Vis DR) spectra in absorbance mode were recorded using a Jasco V 650 spectrometer with an integrating sphere, in the wavelength range of 200–900 nm. TEM images were obtained in a JEOL Model JEM-1200 EXII System, working voltage: 120 kV. A small drop of the dispersion (sample in

water-ethanol 50% solution) was deposited on copper grid and then evaporated in air at room temperature. Room temperature magnetization curves were measured in a vibrating sample magnetometer (VSM) LakeShore 7300, with static field up to $\mu_0 H = 1$ T. Magnetization *vs.* temperature curves were measured in a Quantum Design SQUID magnetometer up to 6 T. The hysteresis properties as coercivity and remanence were obtained directly from the magnetization curves; these hysteresis curves were well fitted by the sum of three contributions: a linear paramagnetic or diamagnetic contribution (LM), a ferromagnetic one (FM), and a superparamagnetic-like one (SPM) [27], so that the total magnetization results: TM = LM + FM + SPM, with:

$$LM = \chi \mu_0 H \tag{1}$$

$$FM = \frac{2M_{SF}}{\pi}\left(\tan^{-1}\right)\left(\frac{H+\mu_0 H_C}{\mu_0 H_C}\right)\tan\frac{\pi M_{RF}}{M_{SF}} \tag{2}$$

$$SPM = M_{SS}\left(\coth\frac{\mu_{SP}H}{K_B T} - \frac{K_B T}{\mu_{SP}H}\right) \tag{3}$$

Here $\mu_0 H_C$, M_{SF}, and M_{RF} are the coercive field and the effective saturation and remanent magnetic moments, associated to the ferromagnetic contribution, respectively. M_{SS}, is the effective saturation magnetic moment and μ_{SP} is the mean magnetic moment of the superparamagnetic units [27]. The temperature dependence of the magnetization was measured following the conventional zero field cooling (ZFC) and field cooling (FC) protocols, under a small applied field of 10 mT.

3. Results and discussion

In a first place, it is important to note that in previous reports we presented the synthesis and characterization of MCM-41 silicates modified with several Fe and Co loadings by the WI method [23,24]. In this study only the solids that showed superparamagnetic behavior were chosen to be tested as host for drug delivery systems.

In addition, this work also includes the synthesis, characterization and analysis of MCM-41 solids modified with iron by DI, in order to compare their properties as drug delivery systems with those of solids synthesized by WI.

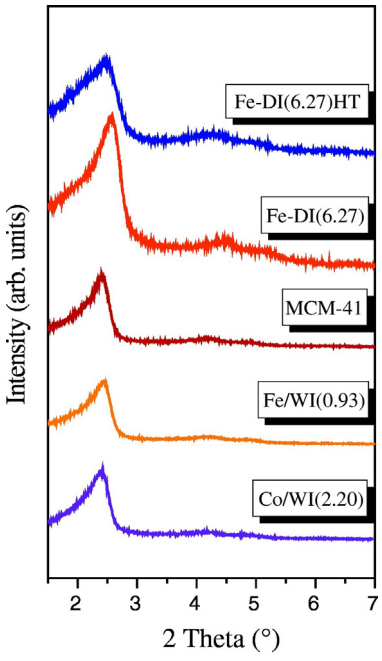

Fig. 1. Low-angle XRD patterns of the synthesized samples by DI and WI methods.

All samples exhibit in their XRD patterns (Fig. 1) a peak at low angle ($2\theta = 2.49$ to $2.59°$) and two lower intensity peaks at $2\theta < 10°$, corresponding to an one-dimensional hexagonal arrangement of channels typical of MCM-41 structure [28–32]. For its part, the lack of peaks in the XRD patterns at high angle for all samples is evidencing that if the oxide nanospecies are present, they are amorphous or their crystal domain size is below the XRD detection limit.

The N_2 adsorption-desorption isotherms of all samples are shown in Fig. 2A. For comparison, the curves have been shifted in the y-axis. The materials exhibit type IV isotherms with an inflection at relative pressures of $P/P^0 \sim 0.1$–0.25 characteristic of capillary condensation inside the conventional mesopores present in MCM-41 structure, called primary mesopores [33–34]. One characteristic of the type IV isotherms is the possible presence of hysteresis loops, which are related with the shape and size of the pores in the adsorbent [35], so that the type of hysteresis loop will depend on the mesoporous structure. In fact, a pronounced hysteresis loop that resemble H4-type according to the IUPAC classification with a sharp decrease in the desorption branch at $P/P^0 \sim 0.45$–0.5, is observed for the Fe-DI(6.27) sample (without hydrothermal treatment). This feature may be related to the presence of ink-bottle pores [36]. It is notable that when hydrothermal treatment was applied (Fe-DI(6.27)HT), the shape of the hysteresis loop changed. Thus, the hydrothermal treatment allowed the formation of more uniform pores in shape, similar to those of pure silica matrix. Moreover, all samples synthetized by DI method exhibited an increase in the adsorption branch at $P/P^0 \sim 0.80$–0.85 which is usually associated to capillary condensation in secondary mesopores, generally interstitial pores. Although the genesis of secondary mesopores is not fully understood it has been reported that a change in micellar size, caused by the presence of metal species in the synthesis medium, could favor the formation of aggregates more complex than the cylindrical micelles [37]. These aggregates would be responsible for the construction of such mesoporosity. Thus, as it was reported for other metals, a certain amount of iron in the synthesis gel can interfere with the micelle formation, changing the ionic strength and resulting in these complex aggregates [38]. Meanwhile, the isotherms of the MCM-41 matrix and those corresponding to the samples modified by WI are reversible (narrow hysteresis loops), evidencing the presence of highly uniform cylindrical pores [36]. As it is shown in Fig. 2B, all the samples have a narrow pore diameter distribution corresponding to the primary mesoporous range. However, for samples modified by DI, the curves of pore diameter distribution became slightly wider. Moreover, a small increase in the average pore size (Table 1) was also observed when the hydrothermal treatment was applied, which is consistent with the higher incorporation of the heteroatom in the framework. This could also be the reason of the a_0 parameter increase for this sample [33]. Furthermore, Table 1 shows that the samples modified by the WI method have specific area similar to that of pure matrix. Meanwhile samples modified by DI method present smaller areas. This fact could give account for the realignment of the mesoporous structure caused by the presence of the metal incorporated into synthesis gel that results in a decreasing in the specific area.

Fig. 3 shows UV–Vis DR spectra of all samples. The strong absorption around 260 nm indicates the incorporation of metal into the framework for the sample synthesized with Fe by DI [38–41]. As it was claimed by us in a previous report [33] the iron, in the samples modified by DI method, is mostly incorporated into the framework in tetrahedral coordination during synthesis. Then, during the calcination process, the migration of these iron ions may occur from within the framework to the wall of the pores or onto the external surface, forming oxide nanoparticles or nanoclusters. Then, although they were not observed by XRD at high angle, the absorption extending to longer wavelengths for the sample synthesized by DI without hydrothermal treatment would be giving evidence of the presence of larger nanoparticles [41]. Meanwhile, then, the hydrothermal treatment seems to favor the incorporation and stabilization of iron ions within the mesoporous framework, reducing their

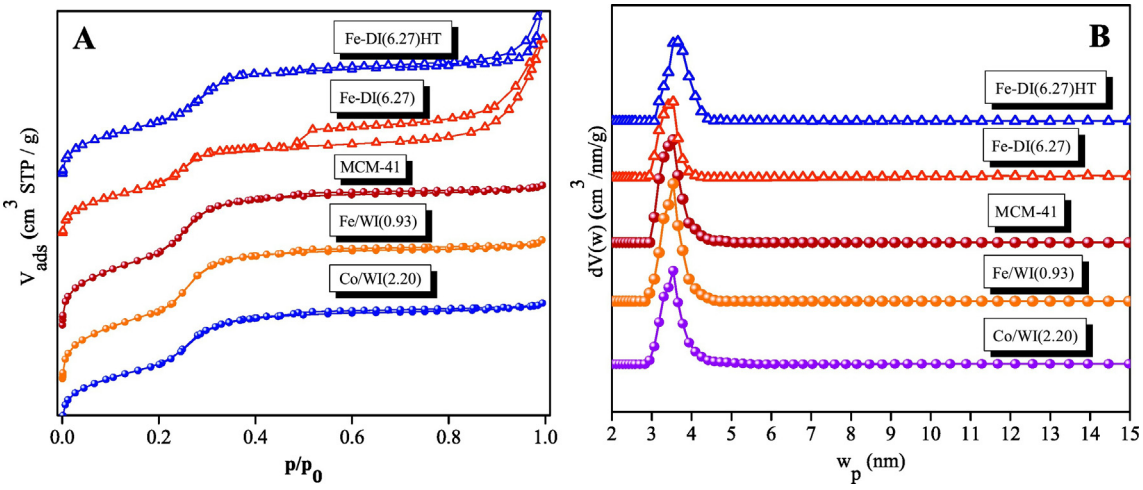

Fig. 2. A) Nitrogen adsorption-desorption isotherms and B) Pore size distribution curves of the samples synthesized by DI and WI methods.

mobility during calcination and subsequent segregation as oxides [33]. This is evidenced by the increase in the intensity of the absorption at 260 nm and the decrease in the absorption at longer wavelengths, besides the increase in the lattice parameter a_0 already observed for the Fe-DI(6.27)HT in comparison with the Fe-DI(6.27) (Table 1).

On the other hand, samples modified with Fe and Co by WI method have been analyzed by UV–Vis RD previously [23,24]. For these samples, the band at 260 nm could be associated with the dπ-pπ charge transfer between the metal ion and O respectively, indicating that some metal atoms are able to link to surface O atoms, being incorporated onto the host as isolated metal cations [38]. Meanwhile, contributions to longer wavelengths show that iron as cobalt are also present in octahedral coordination in extra-framework positions as nanoclusters or nanoparticles [38–41].

Finally, considering the samples modified with Fe by the two methods (see Fig. 3) it is evident that the samples showed similar spectra despite using different methods and loading of metal. This observation allows inferring that, although the sample modified by DI has iron content higher than the one modified by WI, the iron oxide nanospecies generated in them remained very small and widely dispersed on the surface.

In this study, transmission electron microscopy (TEM) was used to extend the structural analysis presented by XRD and corroborate the presence of nanoclusters and nanoparticles evidenced by UV–Vis DR. It is known that darker areas in TEM images represent the electronically more dense phases and it is possible to consider that metal oxide species are present when irregular contrasts in the images are observed. In Fig. 4B and D a frontal view of the arrangement of mesopores can be seen where the regular order of the channels is preserved without being markedly affected by the presence of metal species. Some pores seem to be filled with the metallic oxides species judging by the very small darker spots with a size of around the pore diameter, evidencing the incorporation of nanoclusters and/or nanoparticles inside the mesopores. Meanwhile, Fig. 4A and C mainly corresponds to views perpendicular to the direction of the pore arrangement and unidirectional straight channels arranged along the long axis. The darker regions along the mesopores are giving account for the incorporation of the nanospecies inside the mesochannels. Thus, metal nanospecies could be stabilized on the surface as very small oxide nanoclusters or nanoparticles, filling the pores. This fact would be evidencing the refiner effect carried out by the support structure, whose pore diameter limits the size of the metal nanospecies formed inside them. This analysis is according to the inferred by XRD and UV–Vis DR.

The magnetic moment curves as a function of applied field at room temperature for all samples are shown in Fig. 5. Given that the incorporated metal (Fe or Co) is the only possible source of magnetic signal, the units of magnetization are Am^2 per kilogram of Metal. From a first observation, it is possible to infer that the modified materials beside a superparamagnetic contribution show a dia-, para-, and even ferromagnetic contribution. Here, in order to make a quantitative analysis the magnetization curves were fitted using the Eqs. (1), (2) and (3), corresponding with the presence of different species already identified in [23,24,33,42]: very small nanoclusters and/or nanoparticles in

Table 1
Structure properties and chemical composition of the synthesized samples.

	Area[a] [m^2/g]	a_o [nm]	Dp[b] [nm]	Ep[c] [nm]	V_{PT} [$cm^3\ g^{-1}$]	Metal content [wt.%][d]
MCM-41	996	4.21	3.5	0.71	0.70	–
Fe/WI(0.93)	996	4.22	3.5	0.72	0.72	0.93
Co/WI(2.20)	862	4.25	3.5	0.75	0.62	2.20
Fe-DI(6.27)	732	4.01	3.5	0.51	0.65	6.27
Fe-DI(6.27)HT	765	4.21	3.7	0.51	0.68	6.27

[a] Determined by BET.
[b] Pore diameter determined by the NLDFT method.
[c] Ep = a_0-Dp.
[d] Determined by ICP.

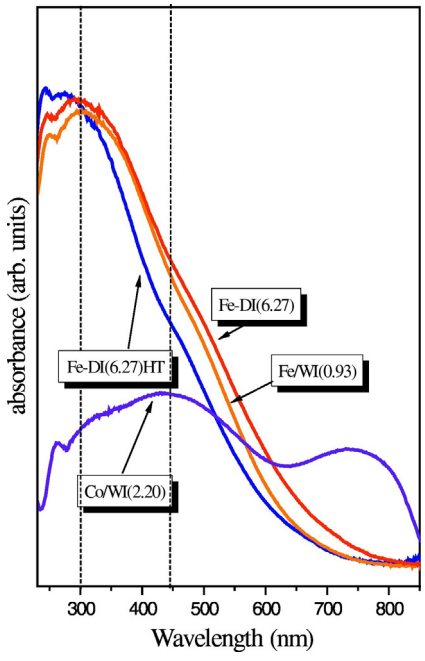

Fig. 3. UV–Vis DR spectra of the samples synthesized by DI and WI methods.

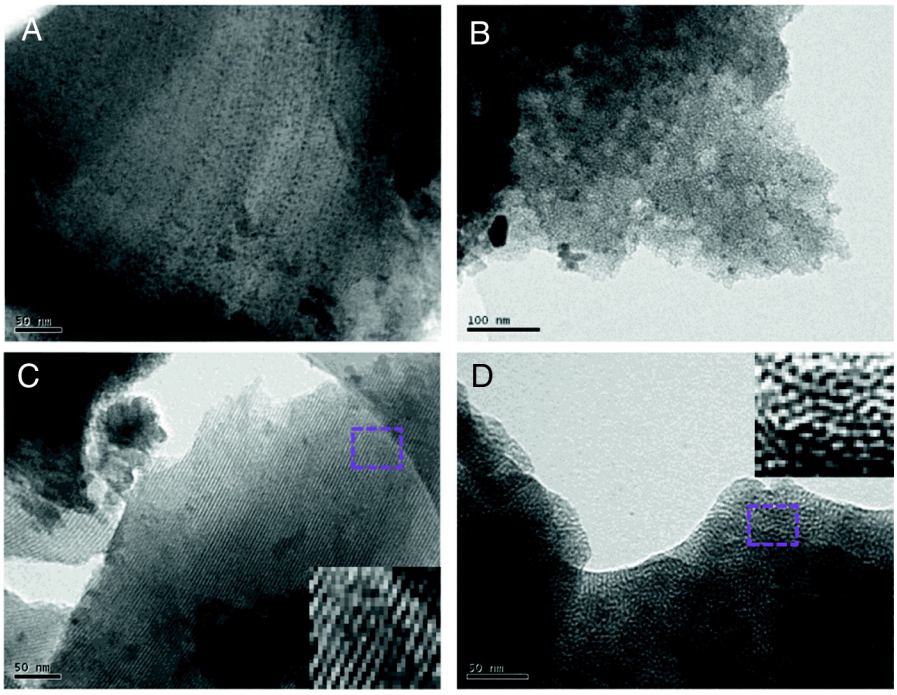

Fig. 4. TEM images of the samples synthesized by DI and WI methods. A) Fe/WI(0.93), B) Co/WI(2.20), C) Fe-DI(6.27) and d) Fe-DI(6.27)HT sample.

superparamagnetic regime (SPM), paramagnetic Fe^{3+} cations incorporated into the walls of the framework (LM) and larger oxides nanoparticles to provide ferromagnetic interactions (FM). The results of these fittings are presented in Table 2. It is noteworthy that the coercivity and remanence are negligible for Fe/WI(0.93) and Fe-DI(6.27)HT samples, and these curves can be fitted only with a superparamagnetic contribution. The low metal content for the sample Fe/WI(0.93) and the refiner effect of the hydrothermal treatment for sample Fe-DI(6.27)HT [33] lead to the formation of very small oxide species, responsible of their superparamagnetic character. Meanwhile, the ferromagnetic contribution observed for Fe-DI(6.27) and Co/WI(2.20) samples probably comes from the oxide nanoparticles of bigger size segregated in the solid. This feature is corroborating the generation of species already inferred by UV–Vis DR.

It is known that silanol groups on the silica surfaces can interact with the carboxyl and benzoyl carbonyl groups of the IND. Therefore, it is very important to know the availability of silanol groups in all samples. For this purpose, the FT-IR spectra of all synthesized samples were recorded after desorption at 400 °C (Fig. 6). It is known that the band at 3740 cm^{-1} indicates the presence of the silanol groups on the structure and that the density of silanol on the surface varies between the different silica materials [43,44]. Here, it is noteworthy that this band is very intense for pure matrix and the iron samples modified by DI method, while it is decreased for the cobalt sample (Co/WI(2.20)) and almost disappears for the iron sample Fe/WI(0.93), both synthesized by WI. In concordance with this, the integrated absorbance of the bands corresponding to the silanol groups was of 1.50, 1.43, 1.30, 0.38, 0.15 for MCM-41, DI(6.27)HT, DI(6.27), Co/WI(2.20), Fe/WI(0.93) samples, respectively. Probably the Si–OH groups could be blocked after the condensation with Fe or Co species, leading to the formation of the Si–O–Fe or Si–O–Co bonds onto the walls and consequently to the lack of the band corresponding to silanol groups [24].

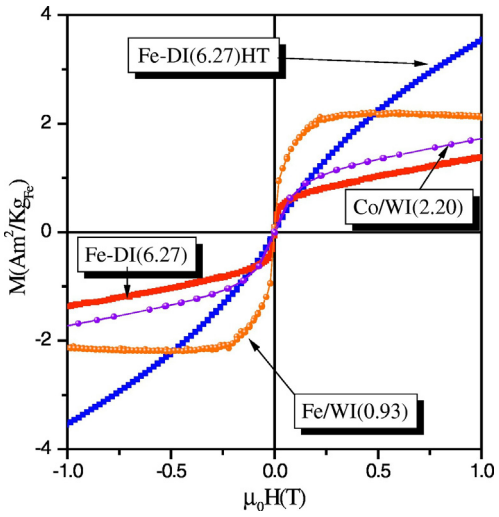

Fig. 5. Curves of magnetization *versus* applied field measured at room temperature for all samples studied in a VSM magnetometer.

To study the behavior of these materials in release systems, IND was incorporated on them and then released in a simulated medium at 37 °C (a temperature close to that of the human body). Thus, the percentages of adsorption of IND in the different mesoporous materials, the percentages of maximal release after 15 min and 8 h of dissolution are presented in Table 3. It is important to note here that measurements of specific surface were performed for the samples before and after the drug loading. A reduction above 60% was observed for the loaded samples, which can be related with a reduction of the total pore volume evidencing the presence of drug inside the channels, as it has already been indicated by others authors [45–47]. Then, the release kinetic of the drug was studied as a function of time and the results for different systems are shown in Fig. 6. It is important to note that although the maximum release of the drug adsorbed on the support occurs before 8 h, it is known that the silicon supports can stay in the body up to 1 day before to be expelled [48]. As it can be seen, the MCM-41 and modified MCM-41 materials exhibit different drug release profiles. It is known that the *in vitro* processes involve a large number of variables, and this fact difficult the fit of them to a particular model. This is the reason why parameters independent of the kinetic models are generally used. Then, the parameters frequently used are: MDT (Mean Dissolution Time) and $t_{50\%}$, both shown in Table 3.

Table 2
Magnetic parameters after fitting to data of Fig. 4.

	M_{SF} $[\frac{Am^2}{kg_{Fe}}]$	M_{RF} $[\frac{mAm^2}{kg_{Fe}}]$	$\mu_0 H_C$ [mT]	M_{SS} $[\frac{Am^2}{kg_{Fe}}]$	μ_{SP} $[\mu_B]$	$\mu_0{}^{\chi}$ $[\frac{Am^2}{T \cdot kg_{Fe}}]$
Fe/WI(0.93)	–	–	–	2.44	15,017	−0.27
Co/WI(2.20)	0.02	30	4.7	1.06	12,000	0.69
Fe-DI(6.27)	0.53	86.7	2.6	0.20	5706	0.76
Fe-DI(6.27)HT	–	–	–	2.20	2384	1.74

M_{SF}: ferromagnetic effective saturation moment, M_{RF}: remanent moment, $\mu_0 H_C$: coercivity field, Mss: superparamagnetic effective saturation momentμ_{SP}: magnetic moment of the superparamagnetic units and $\mu_0{}^{\chi}$: diamagnetic susceptibility.
*Determined by ICP method.
The linear regression coefficient was $R^2 = 0.9999$ for all fitting.

Considering that $t_{50\%}$ is the time when 50% of drug is released, this parameter is calculated by direct interpolation of the curve using the cumulative percentage of drug release *vs* time. Then, MDT is the time needed to dissolve the drug considering that the movement of drug molecules from a solid form to the dissolution medium is governed by the law of statistical probabilities. The average time of dissolution, can be conceived as a frequency distribution with a mean and standard deviation. Thus, the average dissolution time was calculated according to the following expression:

$$MDT = \frac{\Sigma_{i=1}^{n} t \cdot \Delta M_i}{\Sigma_{i=1}^{n} \Delta M_i} \quad (7.1)$$

where, *i* is the number of samples, *n* is the number of samples at time t, *t* is the average between t and (t-1) and ΔMi is the amount dissolved between t and (t-1).

In a first place, it can be observed in Fig. 6 that all modified materials have faster profiles than the bare silica matrix. For its part, these solids also show the lowest values for the $t_{50\%}$ and MDT and the highest values for the maximum release percentage and the release percentage at 15 min (Table 3). This could be due to the presence of nanoparticles and/or clusters of oxides inside channels that might increase the steric diffusion resistance. Thus, the drug could diffuse through the channels of the modified material with less freedom that through those of MCM-41. Therefore, the drug molecules could not penetrate deeply in the structure channels and consequently they are faster released. Moreover, the supports modified by WI method, (Fe/WI(0.93) and Co/WI(2.20)), showed a lower IND adsorption and faster release than samples modified by DI, being the release profile corresponding to Fe/WI(0.93)/IND the fastest of all. This fact is probably due to the lack or decrease in the density of silanol groups capable to interact with the IND, as it was already observed by FT-IR. Finally, it is worth to note that samples modified with iron by DI method (Fe-DI(6.27)and Fe-DI(6.27)HT) have a behavior similar to that of MCM-41. This particular feature could be associated to the presence and availability of silanol groups given by the applied synthesis method (Fig. 7).

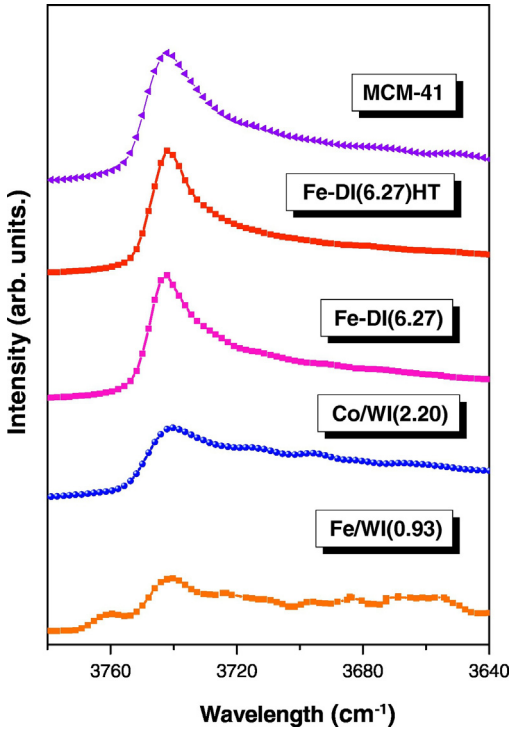

Fig. 6. FTIR spectra of the samples synthesized by DI and WI methods.

In order to perform an exhaustive study of the dissolution kinetics and to obtain the parameters characterizing the process, the mathematical treatment of experimental data have been carried out. In this sense, it is well established that the release kinetics of drugs in biological media from classical forms, are generally governed by a zero order or first order. However, the drug release from ordered mesoporous materials tends to follow the model of Higuchi, but this model is suitable only for a drug release of up to a 50% [49]. Then, in order to find the kinetic mechanism that directs the systems presented here, different models were evaluated, among which the Pepas and Sahlin model was the one that better fitted to the obtained release profiles.

In 1989, Peppas and Sahlin proposed the following biexponential equation which is independent of geometry of delivery system:

$$\%Q = K_1 \cdot t^n + K_2 \cdot t^{2n} \quad (7.6)$$

where *n* is the Fickian diffusion exponent for a system with any geometric shape.

The equation proposed by Peppas and Sahlin is the sum of two terms where the first represents the contribution of Fickian mechanism and the second represents the contribution to the mechanism of relaxation of polymeric chains. Here, when the value of *n* is 0.45, the drug release follows a diffusion mechanism of the Fickian type (or transport Case I). This mechanism of diffusion states that the flux density is proportional to the drug concentration gradient. When the values of *n* are >0.45 and smaller than 1, an abnormal diffusion or non-Fickian occurs; this means that the diffusion rate depends not only on the drug concentration gradient. In the case of $n = 1$ the kinetics of the release system is

Table 3
Percentage of IND adsorption, percentage of maximum release and after 15 min and independent model parameters for all formulations.

	IND adsorption [wt.%]	Max. release [wt.%]	Release at 15 min. [wt.%]	$t_{50\%}$ [min]	MDT [min]
MCM-41/IND	76.50	62.08	12.85	152	10.84
Fe-DI(6.27)/IND	74.56	74.96	15.48	92	10.83
Fe-DI(6.27)HT/IND	78.69	65.30	13.74	149	10.52
Fe/WI(0.93)/IND	57.42	82.37	34.21	32	8.98
Co/WI(2.20)/IND	64.81	73.07	32.46	62	9.41
Indomethacin	–	56.73	17.41	180	–

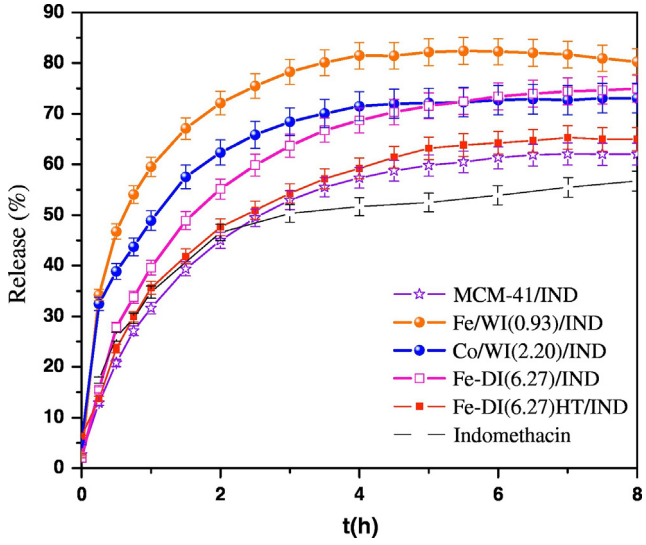

Fig. 7. Profile of IND release for all formulations.

zero order (transport Case II) [50]. The results of applying this model to the experimental data obtained using the mesoporous materials presented here as adsorbents, are shown in Table 4.

It is noted that the linear regression coefficient is quite good even though this model was designed to inflatable polymeric supports. However, for these mesoporous silica systems, a second constant is required due to a gradual and progressive decrease in the drug diffusion process rate over time. This decrease in rate reveals that the drug is firstly released from the external surface and then from the inside of the pores. Thus, when the process progresses and the drug molecules must be released from channels depth, such release process is delayed.

The fact that the fitting values were $n \sim 0.6$ (Table 4) for formulations of MCM-41/IND, Fe-DI(6.27)/IND and Fe-DI(6.27)HT/IND indicates an anomalous diffusion or non-Fickian diffusion for these solids, probably due to the existing interaction between silanol groups of the materials and the drug molecule. On the other hand, the values of $n \sim 0.45$ for Fe/WI(0.93)/IND and Co/WI(2.20)/IND are consistent with a predominance of Fickian diffusion mechanism, which indicates a low or non-existent chemical interaction between the active substance and solids.

According to the statement above it is expected that the samples with $n > 0.45$ possess greater number of available silanol groups. This fact was confirmed by FT-IR for MCM-41/IND, Fe-DI(6.27)/IND, Fe-DI(6.27)HT/IND samples, explaining the slower drug release. Meanwhile for the mesoporous materials modified by the WI method, which do not present available silanols, "n" was <0.45, indicating that the Fickian diffusion is predominant and the simple diffusion of drug molecules through the pores is the limiting step. Thus, the diffusion of the drug molecules from the pores is largely dependent on the nature of the interaction of the drug molecule with the pore wall and the intrinsic mobility of the drug molecules inside the pores. In the case of materials modified by DI method, the presence of greater amount of the silanol groups on the surface causes greater interaction and consequently the diffusion deviates from the Fick's law.

Table 4
Fitting parameters obtained from the Peppas y Sahlin equation.

	Regression coefficient (R^2)	Kinetic constant (K_1)	Kinetic constant (K_2)	n
MCM-41/IND	0.99774	37.02	−5.51	0.64
Fe-DI(6.27)/IND	0.99739	46.55	−7.27	0.61
Fe-DI(6.27)HT/IND	0.99195	40.25	−6.22	0.60
Fe/WI(0.93)/IND	0.99864	76.70	−17.76	0.45
Co/WI(2.20)/IND	0.99361	64.40	−14.14	0.45

4. Conclusions

Superparamagnetic nanocomposites from modified MCM-41 were successfully synthesized by wet impregnation and direct incorporation method. It was possible to incorporate Indomethacin into all selected host materials, and their adsorption capacities and release properties were evaluated. All formulations showed release rate higher than that of pure matrix, due to the oxide nanoparticles and nanoclusters present in the pores hinders the penetration of the drug molecule. It was also observed that the materials modified by WI showed a decreased adsorption capacity and an increased release rate due to a reduced availability of silanol groups which are capable to interact with drug molecules. This leads to that the dominant diffusion mechanism for these samples is the Fickian diffusion type. In addition, materials modified by DI method (as confirmed by FT-IR spectroscopy) have increased availability of silanol groups, which can form hydrogen bridge bonds with carboxyl and carbonyl groups of indomethacin. This would explain their higher drug adsorption capacity and the slower drug release rate. Then, these solids seem to be the most appropriate for the purpose of study of this work. These formulations have good properties of adsorption and release, similar to that of the parent pure MCM-41 and simultaneously their modification with iron nanospecies leads to materials with the superparamagnetic behavior researched.

Acknowledgements

The authors are grateful to CONICET, UTN-FRC and FaMAF-UNC for the financial support.

References

[1] J. Yoo, C. Lee, Drug delivery systems for hormone therapy, J. Control. Release 112 (2006) 1–14.
[2] M. Malmsten, Soft drug delivery systems, Soft Mater. 2 (2006) 760–769.
[3] M. Vallet-Regí, Ordered mesoporous materials in the context of drug delivery systems and bone tissue engineering, Chem. Eur. J. 12 (2006) 5934–5943.
[4] Q. Pankhurst, J. Connolly, S. Jones, J. Dobson, Applications of magnetic nanoparticles in biomedicine, J. Phys. D. Appl. Phys. 36 (2003) R167–R181.
[5] P. Horcajada, C. Márquez-Alvarez, A. Rámila, J. Pérez-Pariente, M. Vallet-Regí, Controlled release of ibuprofen from dealuminated faujasites, Solid State Sci. 8 (2006) 1459–1465.
[6] J. Andersson, J. Rosenholm, S. Areva, M. Lindén, Influences of material characteristics on ibuprofen drug loading and release profiles from ordered micro-and mesoporous silica matrices, Chem. Mater. 16 (2004) 4160–4167.
[7] Y. Zhu, J. Shi, Y. Li, H. Chen, W. Shen, P. Dong, Storage and release of ibuprofen drug molecules in hollow mesoporous silica spheres with modified pore surface, Micropor. Mesopor. Mat. 85 (2005) 75–81.
[8] C. Kresge, M. Leonowicz, W. Roth, J. Vartuli, J. Beck, Ordered mesoporous molecular sieves synthesized by a liquid-crystal template mechanism, Nature 359 (1992) 710–712.
[9] J. Beck, J. Vartuli, W. Roth, M. Leonowicz, C. Kresge, K. Schmitt, C. Chu, D. Olson, E. Sheppard, S. McCullen, J. Higgins, J. Schlenker, A new family of mesoporous molecular sieves prepared with liquid crystal templates, J. Am. Chem. Soc. 114 (1992) 10834–10843.
[10] M. Vallet-Regi, F. Balas, D. Arcos, Mesoporous materials for drug delivery, Angew. Chem. Int. Ed. 46 (2007) 7548–7558.
[11] N. Botterhuis, Q. Sun, P. Magusin, R. Santen, N. Sommerdijk, Hollow silica spheres with an ordered pore structure and their application in controlled release studies, Chem. Eur. J. 12 (2006) 1448–1456.
[12] Q. Pankhurst, J. Connolly, S. Jones, J. Dobson, Applications of magnetic nanoparticles in biomedicine, J. Phys. D. Appl. Phys. 36 (2003) 167–181.
[13] Q. Yang, S. Wang, P. Fan, L. Wang, Y. Di, K. Lin, F. Xiao, pH-Reponsive carrier system based on carboxylic acid modified mesoporous silica and polyelectrolyte for drug delivery, Chem. Mater. 17 (2005) 5999–6003.
[14] S. Giri, B. Trewyn, M. Stellmaker, V. Lin, Stimuli-responsive controlled-release delivery system based on mesoporous silica Nanorods capped with magnetic nanoparticles, Angew. Chem. Int. Ed. Engl. 44 (2005) 5038–5044.
[15] L.T. Canhamlt, Bioactive silicon structure fabrication through nanoetching techniques, Adv. Mater. 7 (1995) 1033–1035.
[16] S.H.C. Anderson, H. Elliot, D.J. Wallis, L.T. Canhamlt, J.J. Powell, Dissolution of different forms of partially porous silicon wafers under simulated physiological conditions, Phys. Status Solidi A 197 (2) (2003) 331–335.
[17] D.M. Refitt, R. Jugdaohsinghr, R.P. Thompson, J.J. Powell, Silicic acid: its gastrointestinal uptake and urinary excretion in man and effects on aluminium excretion, J. Inorg. Biochem. 76 (1999) 141–147.
[18] A. Rosengren, L. Wallman, M. Bengtsson, T.H. Laurell, N. Danielsen, N. Anielsen, L.M. Bjurtsen, Tissue reactions to porous silicon: a comparative biomaterial study, Phys. Status Solidi A 182 (2000) 527–531.

[19] Y. Ou, C. Yang, C. Cheng, S. Raung, Y. Hung, C. Chen, Indomethacin induces apoptosis in 796-O renal cell carcinoma cells by activating mitogen-activated protein kinases and AKT, Eur. J. Pharmacol. 563 (2007) 49–60.
[20] J. Qin, J. Yuan, L. Li, H. Liu, R. Qin, W. Qin, In vitro and in vivo inhibitory effect evaluation of cyclooxygenase-2 inhibitors, antisense cyclooxygenase-2 cDNA, and their combination on the growth of human bladder cancer cells, Biomed. Pharmacother. 63 (2009) 241–248.
[21] T. Orido, H. Fujino, T. Kawashima, T. Murayama, Decrease in uptake of arachidonic acid by indomethacin in LS174T human colon cancer cells; a novel cyclooxygenase-2-inhibition-independent effect, Arch. Biochem. Biophys. 494 (2010) 78–85.
[22] V. Elías, M. Crivello, E. Herrero, S. Casuscelli, G. Eimer, Some considerations to optimize the synthesis procedure and the structural quality of mesostructured silicas, J. Non-Cryst. Solids 355 (2009) 1269–1273.
[23] N. Cuello, V. Elías, M. Crivello, M. Oliva, G. Eimer, Synthesis, characterization and magnetic behavior of Co/MCM-41nanocomposites, J. Solid State Chem. 205 (2013) 91–96.
[24] N. Cuello, V. Elías, C. Rodriguez Torres, M. Crivello, M. Oliva, G. Eimer, Development of iron modified MCM-41 as promising nanocomposites with specific magnetic behavior, Micropor. Mesopor. Mat. 203 (2015) 106–115.
[25] T. Kokubo, H. Kushitani, S. Sakka, T. Kitsugi, T. Yamamuro, Solutions able to reproduce in vivo surfacestructure changes in bioactive glass-ceramic A-W, J. Biomed. Mater. Res. 24 (1990) 721–734.
[26] J. Villarroel Rocha, D. Barrera, K. Sapag, Improvement in the pore size distribution for ordered mesoporous materials with cylindrical and spherical pores using the kelvin equation, Top. Catal. 54 (2011) 121–134.
[27] M. Stearns, Cheng. Y. Determination of para- and ferromagnetic components of magnetization and magnetoresistance of granular Co/Ag films, J. Appl. Phys. 75 (1994) 6894–6898.
[28] V. Elías, M. Crivello, E. Herrero, S. Casuscelli, G. Eimer, Some considerations to optimize the synthesis procedure and the structural quality of mesos-tructured silicas, J. Non-Cryst. Solids 355 (2009) 1269–1273.
[29] A. Patterson, The Scherrer formula for X-ray particle size determination, Phys. Rev. 56 (1939) 978–982.
[30] H. Klug, L. Alexander, X-ray Diffraction Procedures for Polycrystalline and Amorphous Materials, second ed. John Wileyand Sons, New York, 1974.
[31] X. Hao, Y. Zhang, J. Wang, W. Zhou, C. Zhang, S. Liu, A novel approach to prepare MCM-41 supported CuO catalyst with high metal loading and dispersion, Micropor. Mesopor. Mat. 88 (2006) 38–47.
[32] S. Aspromonte, A. Sastre, A. Boix, M. Cocero, E. Alonso, Micropor. Mesopor. Mat. 148 (2012) 53–61.
[33] N. Cuello, V. Elías, S. Urreta, M. Oliva, G. Eimer, Microstructure and magnetic properties of iron modified mesoporous silica obtained by one step direct synthesis, Mater. Res. Bull. 48 (2013) 3559–3563.
[34] K. Sing, D. Everett, R. Haul, L. Moscou, R. Pierotti, J. Rouquerol, T. Siemieniewska, Reporting physisorption data for gas/solid systems, Pure Appl. Chem. 57 (1985) 603–619.
[35] J. Martínez, Adsorción física de gases y vapores por carbones. Secretariado de Publicaciones de la Universidad de Alicante, ISBN: 84-86809-33-9, 2017.
[36] F. Rouquerol, J. Rouquerol, K. Sing, Adsorption by Powders and Porous Solids. Principles, Methodology and Applications, Academic Press, New York, 1999.
[37] I. Díaz, J. Pérez-Pariente, Synthesis of spongelike functionalized MCM-41 materials from gels containing amino acids, Chem. Mater. 14 (2002) 4641–4646.
[38] G. Eimer, C. Chanquia, K. Sapag, E. Herrero, The role of different parameters of synthesis in the final structure of Ti-containing mesoporous materials, Micropor. Mesopor. Mat. 116 (2008) 670–676.
[39] Y. Wang, Q. Zhang, T. Shishido, K. Takehira, Characterizations of iron-containing MCM-41 and its catalytic properties in epoxidation of styrene with hydrogen peroxide, J. Catal. 209 (2002) 186–196.
[40] S. Liu, Q. Wang, P. Van Der Voort, P. Cool, Magnetism of iron-containing MCM-41 spheres, J. Magn. Magn. Mater. 280 (2004) 31–36.
[41] D. Beydoun, R. Amal, G. Low, S. MacEvoy, Role of nanoparticles in Photocatalysis, Nanopart. J. Res. 1 (1999) 439–458.
[42] N. Cuello, Elías, E. Winkler, G. Pozo-López, M. Oliva, G. Eimer, Magnetic behaviorofiron-modified MCM-41correlated with Clustering processes from the wet impregnation method, J. Magn. Magn. Mater. 407 (2016) 299–307.
[43] M. Manzano, V. Aina, C. Arean, F. Balas, V. Cauda, M. Colilla, M. Delgado, Vallet-Regí. M. Studies on MCM-41 mesoporous silica for drug delivery: effect of particle morphology and amine functionalization, Chem. Eng. J. 137 (2008) 30–37.
[44] Heikkila Limnell, Santos, Sistonen, Hellsten, Laaksonen, Peltonen, Kumar, Murzin, Louhi-Kultanen, Salonen, Hirvonen, Lehto physicochemical stability of high indomethacin payload ordered mesoporous silica MCM-41 and SBA-15 microparticles, Int. J. Pharm. 416 (2011) 242–251.
[45] J. Andersson, J. Rosenholm, S. Areva, M. Lindén, Influences of material characteristics on ibuprofen drug loading and release profiles from ordered micro- and mesoporous silica matrices, Chem. Mater. 16 (2004) 4160–4167.
[46] M. Vallet-Regi, A. Rámila, R.P. del Real, J. Pérez-Pariente, A new property of MCM-41: drug delivery system, Chem. Mater. 13 (2001) 308–311.
[47] P. Horcajada, A. Rámila, J. Pérez-Pariente, M. Vallet-Regi, Influence of pore size of MCM-41 matrices on drug delivery rate, Micropor. Mesopor. Mat. 68 (2004) 105–109.
[48] E. Pastor, E. Matveeva, A. Valle-Gallego, F. Goycoole, M. Garcia-Fuentes, Protein delivery based on uncoated and chitosan-coated mesoporous silicon microparticles, Colloids Surf. B: Biointerfaces 88 (2011) 601–609.
[49] T. Higuchi, Mechanism of sustained-action medication. Theoretical analysis of rate of release of solid drugs dispersed in solid matrices, Pharm. Sci. 52 (1963) 1145–1149.
[50] P. Ritger, N. Peppas, A simple equation for description of solute release I. Fickian and non-Fickian release from of slabs, spheres, cylinders or discs, J. Control. Release 5 (1987) 23–36.